Electronic Supporting Information (ESI)

All-Nanoparticle Layer-by-layer Coatings for Mid-IR On-Chip Gas Sensing

Diana Al Husseini,[a] Junchao Zhou,[b] Daniel Willhelm,[a] Trevor Hastings,[a] Gregory S. Day,[c] Hong-Cai Zhou,[a,c] Gerard L. Coté,[d] Xiaofeng Qian,[a] Ricardo Gutierrez-Osuna,[e] Pao Tai Lin[a,b] and Svetlana A. Sukhishvili*[a]

a. Department of Materials Science and Engineering, Texas A&M University, College Station, TX 77843

b. Department of Electrical and Computer Engineering, Texas A&M University, College Station, TX 77843

c. Department of Chemistry, Texas A&M University, College Station, TX 77843

d. Department of Biomedical Engineering, Texas A&M University, College Station, TX 77843

e. Department of Computer Science and Engineering, Texas A&M University, College Station, TX 77843

* Email: svetlana@tamu.edu

Experimental Section

Materials

Zinc acetate dihydrate (ACS reagent, ≥ 98%) and hydrogen peroxide solution (30 wt. % in H_2O, ACS reagent) for zinc peroxide nanoparticles (NPs) synthesis were purchased from Sigma Aldrich. LUDOX TM-40 colloidal silica (40 wt. % suspension in H_2O) was purchased from Sigma Aldrich. Ultrapure Milli-Q water (deionized, DI) (Millipore) with a resistivity of 18.2 MΩ/cm was used in all experiments. All materials were used as received with no further purification. Silicon wafers (100 orientation, P/B doped) were purchased from Wafer Pro Inc.

Dipping solution conditions:

ZnO_2 and SiO_2 aqueous solutions were prepared at concentrations of 0.2 wt.% with pH of 5.5 and 10, respectively. DI water was utilized for dilution purposes. The pH of the solutions did not require further adjustment after dilution.

Silicon wafers cleaning method

Before use, wafers were precleaned using ultraviolet (UV) light and concentrated sulfuric acid to remove organic contaminants.

Instrumentations

Ellipsometry:

Thickness of the assembled films on silicon substrates were characterized using a J.A Woollam Co., M-2000 spectroscopic ellipsometer. The data analysis was done using the CompleteEASE software package. Measurements were performed at wavelengths from 600 to 1000 nm and at angles 45^o, 55^o and 65^o. The data obtained were fitted using a Cauchy model that is based on the assumption that the real part of the refractive index (n) can be described as follows:

$$n(\lambda) = A + \frac{B}{\lambda^2} + \frac{C}{\lambda^4} ,$$

where A, B and C are constants and λ is the wavelength of the incident light. B and C constants were set to zero. The index of refraction was reported as n (λ) = A.

X-ray diffraction (XRD):

Powder X-ray diffraction patterns were collected using Bruker D8 daVinci instrument fitted with a Cu source and a LynxEye XE detector in Bragg-Brentano (theta-theta mode). Data was collected in the X-ray Diffraction Laboratory in the Department of Chemistry at Texas A&M University.

Dynamic light scattering (DLS):

A Zetasizer Nano ZS was used to measure hydrodynamic diameter of the NPs using dynamic light scattering with non-invasive backscatter (NIBS) optics. The ZS also included a zeta potential analyzer, which was used to measure zeta potential of the NPs using electrophoretic light scattering. Diluted aqueous solutions of both ZnO_2 and SiO_2 NPs were prepared at 0.2 wt. % and pH of 5.5 and 10, respectively. Folded capillary zeta cell cuvettes were used for hydrodynamic diameter and zeta potential measurements of the prepared solutions. Data was collected in the Soft Matter Facility (SoMF) at Texas A&M University.

Transmission electron microscopy (TEM):

The morphology of the NPs was acquired using TEM (JEOL1200 EX at 100 kV). The samples were prepared by casting a drop of NP aqueous solutions on copper square grids (EMS 400-CU). Diluted aqueous solutions of both ZnO_2 and SiO_2 NPs were prepared at 0.2 wt. % and pH of 5.5 and 10, respectively. Excess solution was then removed with a filter paper, and the samples were dried at room temperature for at least 12 hours before TEM imaging. ImageJ software was utilized to process the

average diameter for 200 NPs per NP type. Data was collected in the Microscopy and Imaging Center (MIC) at Texas A&M University.

Scanning electron microscopy (SEM):

The coverage and thickness of the films on the Si wafers were acquired using SEM (JSM-7500F JEOL) instrumentation. The wafers were cut using a diamond pen for cross-sectional SEM imaging. The images were taken using an accelerating voltage of 5 kV and emission current of 10 μA. The working distance for top view imaging was 11 mm while that for cross-sectional imaging was 5 mm. Prior to imaging, samples were sputtered with 2.5 nm Pt/Pd coating to avoid charging and obtain better quality images. Coverage analysis was done using Mathematica 12.0 software. Sample images were binarized automatically with a reference in terms of their grayscale histograms. ImageJ software was utilized to process the average thickness of the films. Data was collected in the Materials Characterization Facility (MCF) at Texas A&M University.

Atomic force microscopy (AFM):

The morphology of 5-BL films was acquired using an AFM (Bruker-Dimension Icon). The films were prepared on a silicon wafer using the method described in the main text. For imaging in dry conditions at room temperature (~22 ^{o}C, ~50% relative humidity), tapping mode was used to scan 1 μm × 1 μm area at a scan rate of 1 Hz with a resolution of 512 scan lines A sharp silicon tip (Nanosensors PPP-NCSTR probe) with the normal stiffness of K_n = 7.4 N/m and a resonance frequency of 160 kHz was used. Data was collected in the Materials Characterization Facility (MCF) at Texas A&M University.

Optical imaging:

The optical images of the assembled films on silicon substrates were taken using a Nikon microscope (model Eclipse Ti2-U) at x100 magnification. Data was collected in the Soft Matter Facility (SoMF) at Texas A&M University.

Gas Adsorption Measurements and Brunauer-Emmett-Teller (BET):

Surface area was determined via the BET method[1] based upon a nitrogen (N_2) adsorption isotherm. The N_2 isotherm was collected at 77 K on a Micromeritics ASAP 2420. Before analysis, the sample was activated at 120 °C for 10 h under high vacuum (<100 μbar) The acetone adsorption measurements were conducted on an ASAP 2020 equipped with a vapor sorption accessory. The acetone used in the experiment was degassed via three freeze-pump-thaw cycles on the instrument followed by three rounds of vacuum distillation prior to use. Vapor sorption was conducted at room temperature with the

temperature maintained via a water bath. The sample was activated at 120 °C for 10 h under high vacuum prior to analysis (<100 μbar).

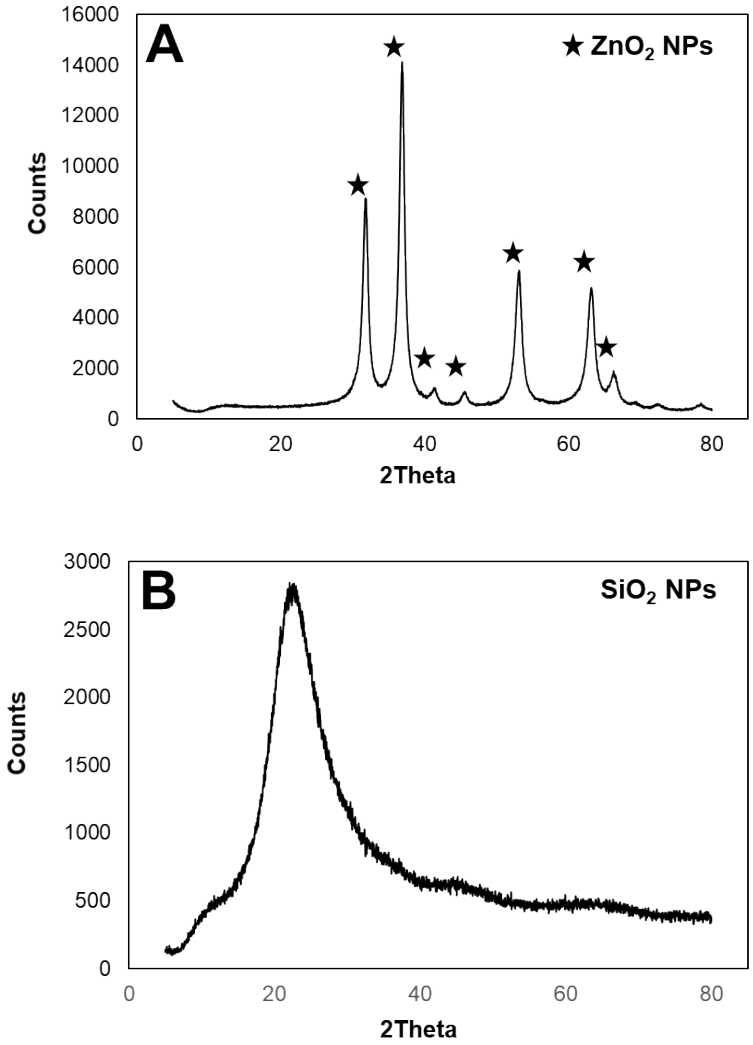

Fig. S1: X-ray diffractogram of ZnO_2 NPs; diffraction peaks associated with the presence of ZnO_2 are as follows: 2Theta values of 31.8, 36.9, 41.5, 45.9, 53.2, 63.3 and 66.3 (A) and SiO_2 NPs (B).

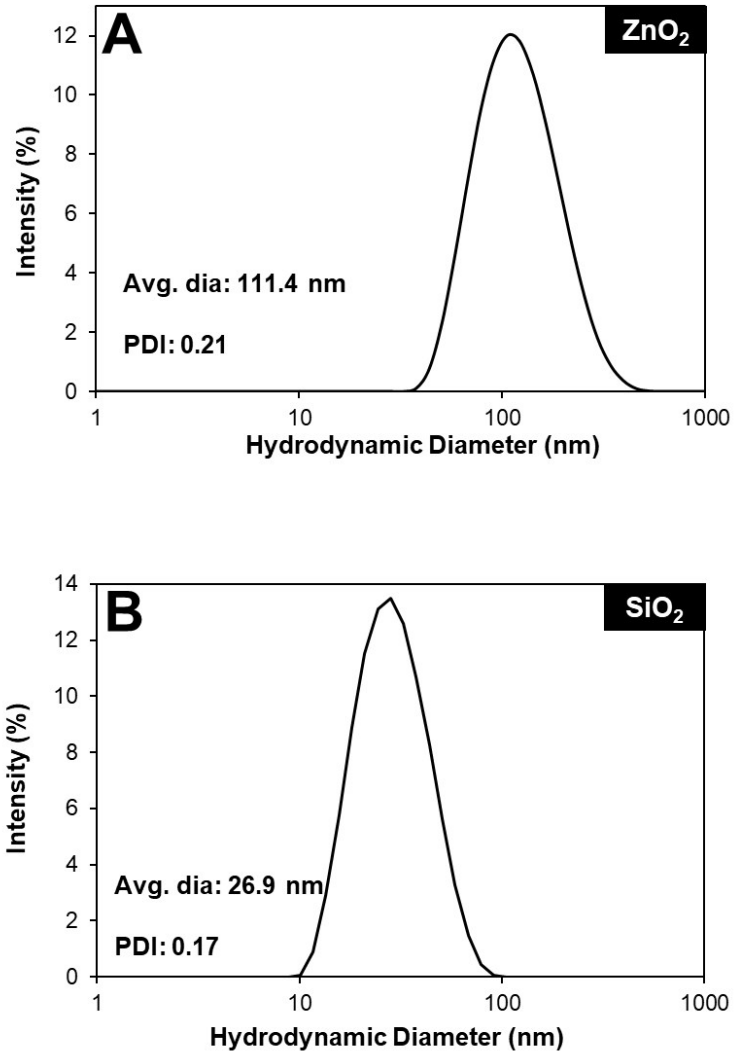

Fig. S2: DLS size distribution of ZnO_2 NPs (A) and SiO_2 NPs (B). *PDI: polydispersity index.

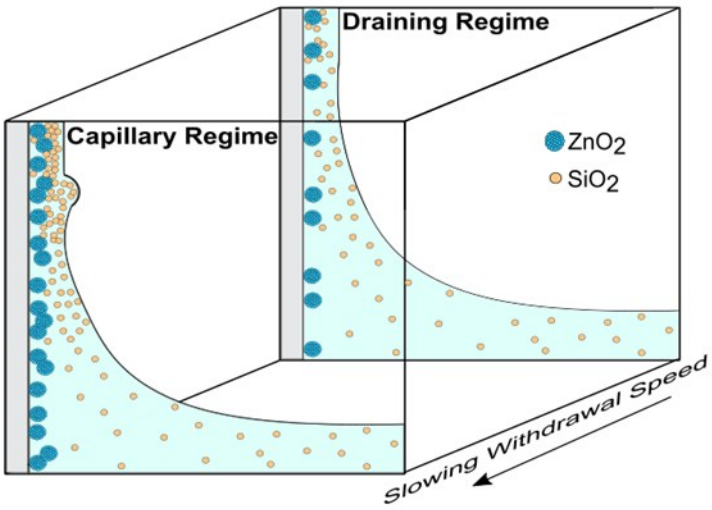

Fig. S3: Illustration showing controlled withdrawal substrate deposition technique.

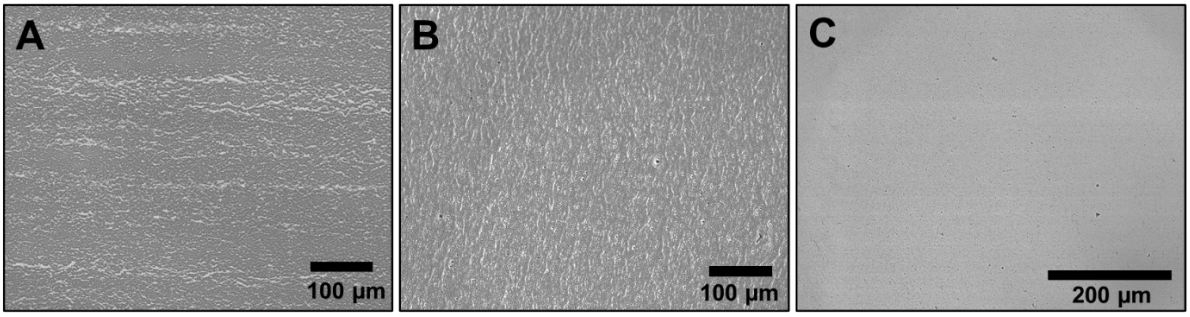

Fig. S4: Optical images of 5-BL thin films using different substrate withdrawal speeds: 0.001 (A), 0.01 (B) and 0.1 cm/sec (C).

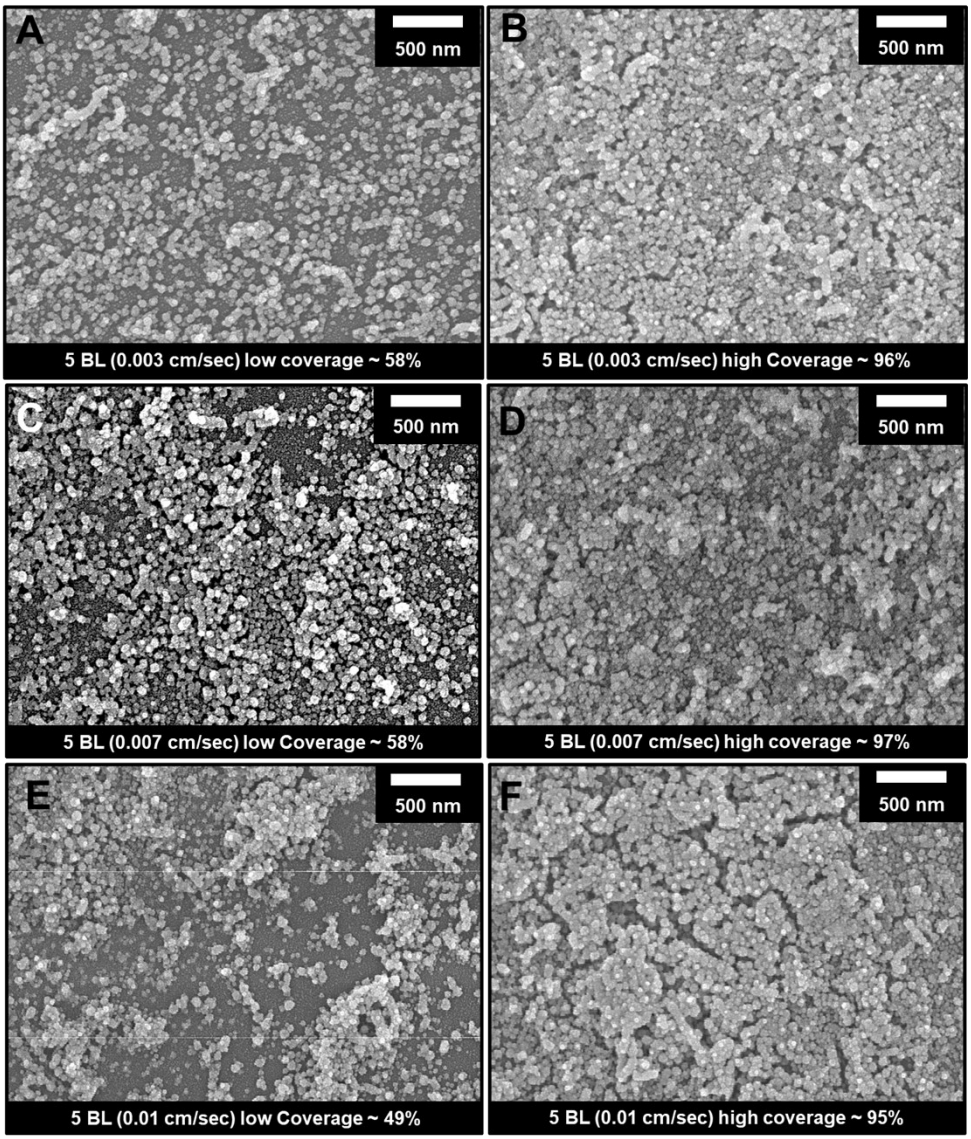
A
500 nm
5 BL (0.003 cm/sec) low coverage ~ 58%
B
500 nm
5 BL (0.003 cm/sec) high Coverage ~ 96%
C
500 nm
5 BL (0.007 cm/sec) low Coverage ~ 58%
D
500 nm
5 BL (0.007 cm/sec) high coverage ~ 97%
E
500 nm
5 BL (0.01 cm/sec) low Coverage ~ 49%
F
500 nm
5 BL (0.01 cm/sec) high coverage ~ 95%

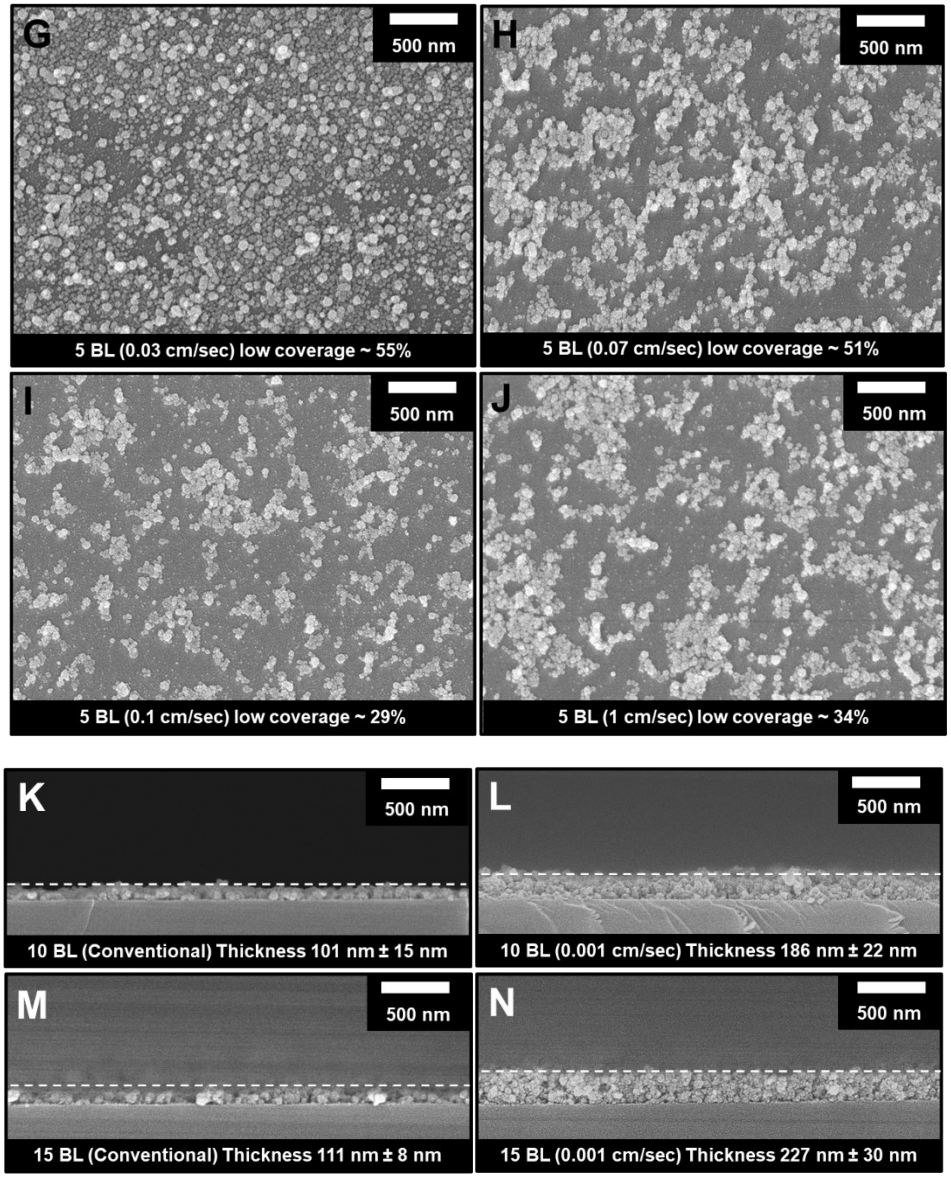

Fig. S5: Top-view SEM images of 5-BL films at different withdrawal speeds. For 0.003 (A and B), 0.007 (C and D) and 0.01 cm/sec (E and F), low and high coverages show non-stripe and stripe areas, respectively, in the films. For 0.03 (G), 0.07 (H), 0.1 (I) and 1 cm/sec (J), the stripe pattern disappears and the low coverage types of films dominate. Coverage analysis was done using Mathematica 12.0 software. All images taken under similar conditions were binarized with the same reference, removing manual biases. Cross-sectional SEM images of 10- and 15-BL films using conventional (K and M) and precisely controlled dipping at 0.001 cm/sec (L and N). Cross-sectional thickness was determined using ImageJ software.

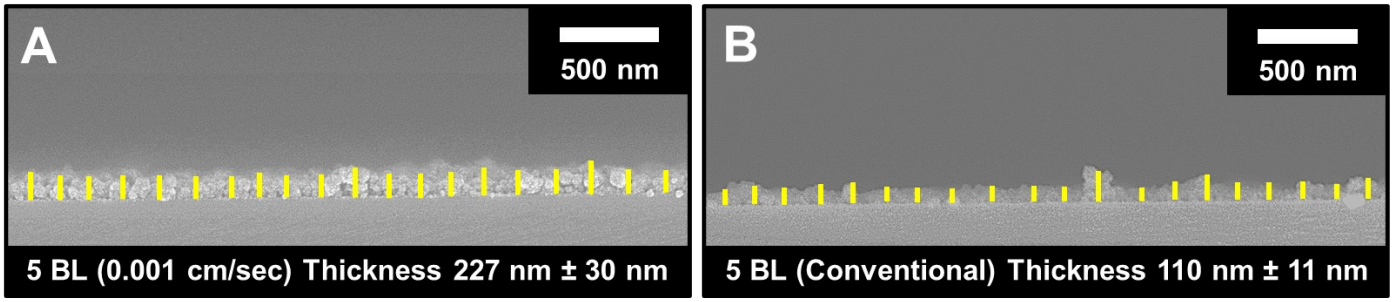

Fig. S6: Cross-sectional SEM images of 5-BL films deposited using precisely controlled dipping at 0.001 cm/sec substrate withdrawal speed (A) and using conventional dipping (B). The illustrated yellow vertical lines were used to estimate the average thickness of both films using Image J software over 20 measurements.

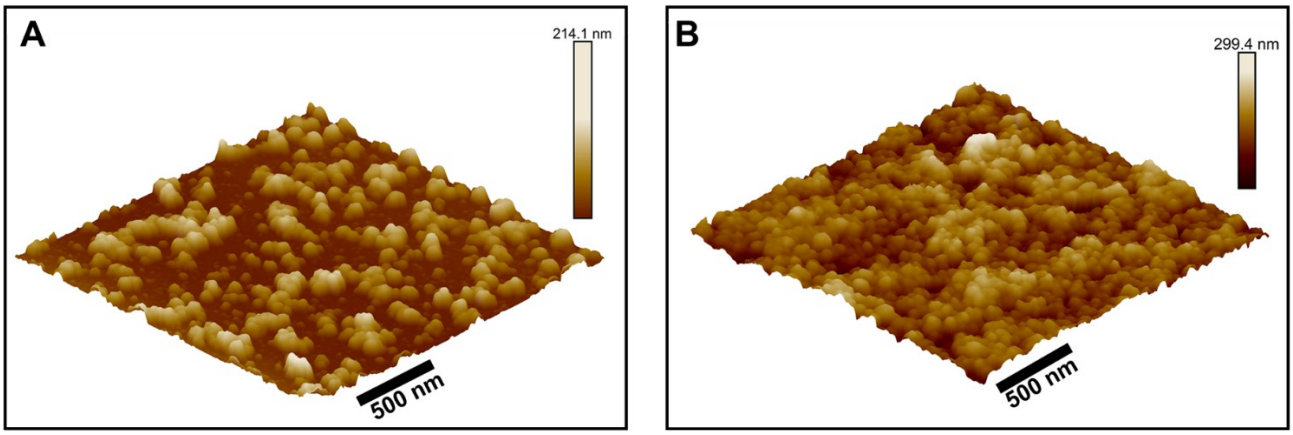

Fig. S7: AFM images of 5-BL films using conventional dipping (A) and precisely controlled dipping at 0.001 cm/sec (B).

Fabrication of a-Si waveguide and PDMS chamber for gas measurements:

A multi-step process consisting of thin film deposition and dry etching was used to fabricate Si waveguides (Fig. S8 A-F). In step A, a 1 µm thick a-Si thin film was deposited on a Si wafer with a 3 µm thermal oxide layer by plasma-enhanced chemical vapor deposition (PECVD). The thermo oxide layer is the low-refractive-index under-cladding layer. In step B, photoresist patterns with the waveguide structure were generated on the top of the a-Si thin film via photolithography. The width of the waveguide was 15 µm. In step C, the waveguide pattern was transferred to the a-Si layer by reactive ion etching (RIE). After removal of the photoresist (step D), 3 µm of SiO_2 layer was deposited on two ends of the a-Si waveguide

and the central region was left open for nanocoating functionalization as shown in step E. This central region interacts with gas molecules. The measured length of the open region is 8 mm long. The top cladding SiO_2 layer was used to protect the waveguide from the subsequent polydimethylsiloxane (PDMS) chamber bonding. Prior to coating deposition, these waveguides were precleaned in an acetone bath for 15 minutes followed by UV light treating for 10 minutes. In the final step F, a PDMS (Dow Corning Sylgard 184) chamber was prepared by loading the PDMS precursor into a 3D-printed mold. The molded PDMS chamber was glued to the waveguide device with uncured PDMS. Once the PDMS was cured, the chamber was completely sealed and its edge was tightly bonded to the waveguide chip. The PDMS chamber is separated from the Si waveguide by the SiO_2 cladding so that the PDMS did not absorb the light from the waveguide. SEM images of the optical waveguides were acquired using SEM (Tescan FERA-3 model) instrumentation at Materials Characterization Facility (MCF), Texas A&M University. The images were taken using an accelerating voltage of 10 kV. The working distance for the top view imaging was 9 mm (Fig. S9).

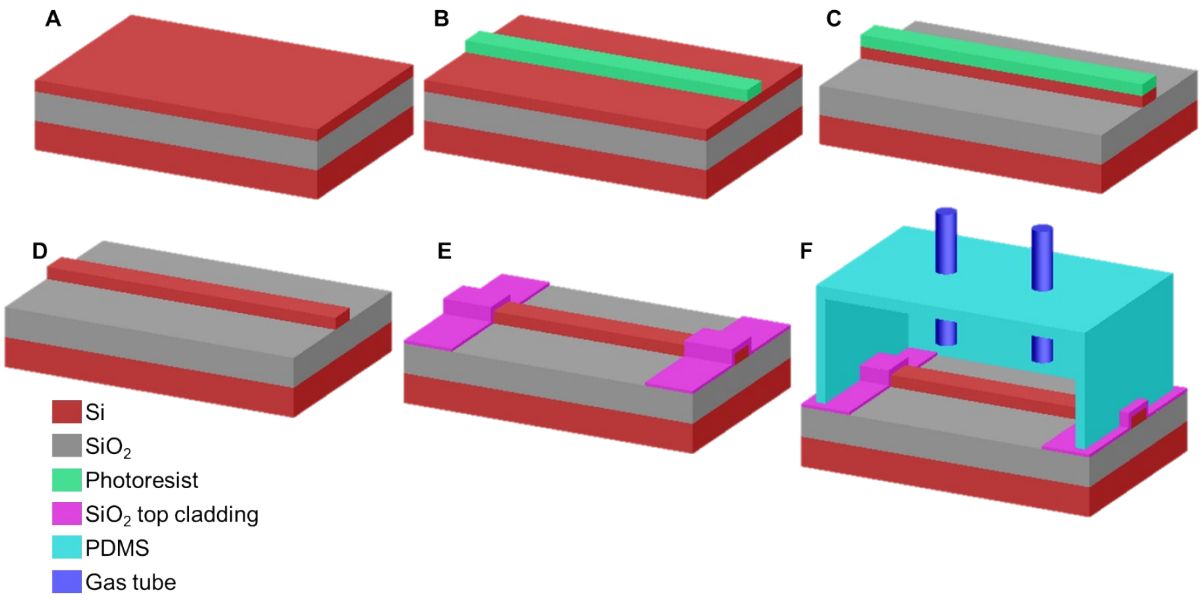

Fig. S8: Schematic showing the fabrication of a-Si waveguide and assembly of the PDMS chamber on the device. a-Si thin film deposition by PECVD (A); Photolithography defined waveguide pattern (B); Pattern transferred to a-Si thin film by RIE (C); Photoresist removed (D); SiO_2 top cladding layer deposited (E); PDMS chamber bonded to the waveguide with gas input and output tubes inserted (F).

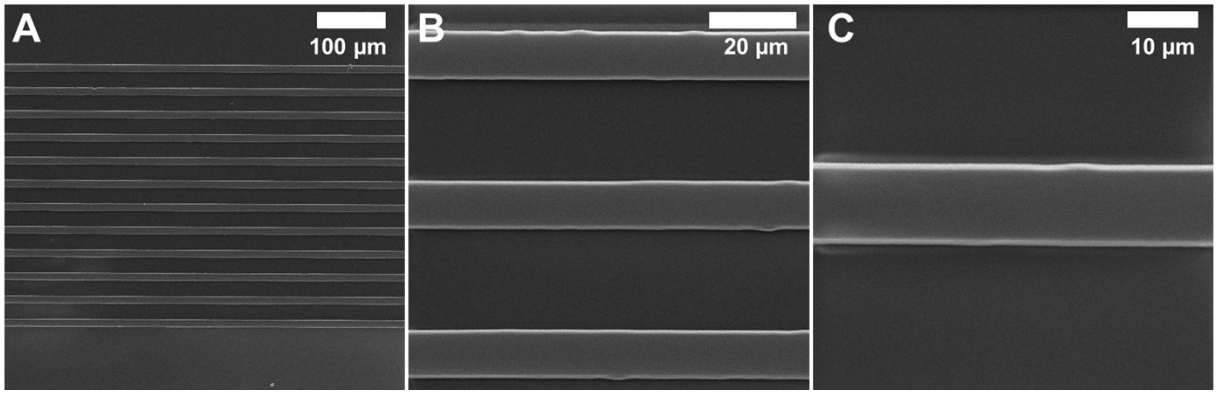

Fig. S9: Top-view SEM images of the optical waveguides at different magnifications (A, B and C).

MIR gas measurement setup:

A tunable MIR laser (M Squared Firefly) with 150 kHz pulse repetition rate, 10 ns pulse duration, and 150 mW average power, was used as the light source. The probe light was collimated into a fluoride fiber with a core diameter of 9 µm by using a reflective lens (RL). The light from the fiber was butt-coupled into the a-Si waveguide. An optical microscope (OM) was used to fine adjust the fiber position. The waveguide mode image was projected to a MIR camera (IRCameras 800 series) by a BaF_2 lens. Nitrogen is used to purge the PDMS chamber since nitrogen is transparent in the mid-IR region. Acetone vapor and pure methane were utilized in these experiments at ambient temperature. Specifically, acetone vapors were obtained by flowing nitrogen through acetone in liquid phase resulting in concentration of 0.72 g/l at ambient temperature (saturated vapors). Two mass flow controllers (MFC) were used to regulate the gas flow rates along the two gas lines. The waveguide light was attenuated by the gas via the evanescent wave absorption at the characteristic MIR absorption wavelengths. The setup is illustrated in Fig. S10.

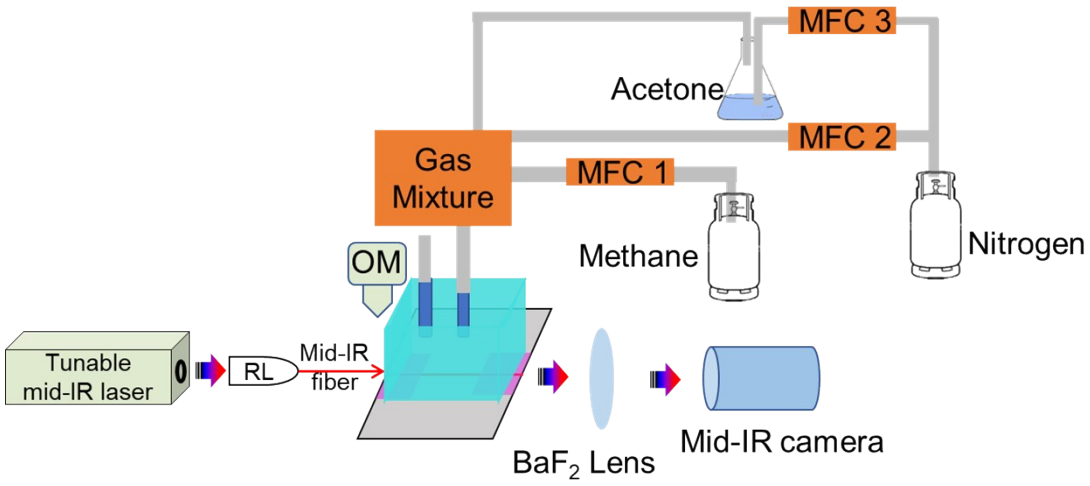

Fig. S10: Schematic showing MIR gas measurement setup.

Computational Details of Surface Adsorption Energy Calculations

First-principles density functional theory (DFT)[1,2] was applied to estimate adsorption energy (E_{ads}) of a single molecule of acetone on the surface of crystalline ZnO_2 and amorphous SiO_2 nanoparticle. A slab model was used to represent the nanoparticle surface. E_{ads} was calculated using $E_{ads} = E_{surface+acetone} - E_{surface} - E_{acetone}$, where $E_{surface+acetone}$ is the total energy of the system containing both the slab (ZnO_2 or SiO_2) and acetone molecule, $E_{surface}$ is the total energy of the slab only (ZnO_2 or SiO_2), and $E_{acetone}$ is the total energy of a free acetone molecule. These quantities were determined from three DFT calculations elaborated below.

The initial crystallographic structure of bulk ZnO_2 (cubic, Pa-3) was obtained from the Materials Project database[3] (*mp-8484*). In our DFT calculations, the acetone molecule was added to the center of a cubic lattice (a=b=c=30 Å). The amorphous SiO_2 was constructed using a combination of molecular dynamics (MD) and DFT – additional details about method are provided below. The DFT calculations for the ZnO_2, SiO_2, and acetone systems were performed using the Vienna ab initio simulation package (VASP).[4,5] We employed the Perdew-Burke-Ernzerhof (PBE) exchange-correlation energy functional within the generalized gradient approximation (GGA)[6]. For relaxation of the bulk and surface slabs, we used the atomic force convergence threshold of 0.02 eV/Å, electronic energy convergence threshold of 10^{-4} eV, and a plane-wave cutoff energy of 520 eV, unless stated otherwise. To minimize the image interaction from the periodic boundary condition in DFT, a vacuum was added to the lattice cell along the z-direction (*i.e.* surface normal), and a dipole correction was applied.[7,8]

The atomic positions and cell parameters of bulk ZnO_2 were fully relaxed using a *k*-point mesh of 7×7×7. After structural relaxation, the lattice constant of bulk ZnO_2 is 4.953 Å. The ZnO_2 surface was then constructed using the Python Materials Genomics (pymatgen) library[9] with a method developed by Sun *et al*.[10] In our calculations, a (100) slab was constructed with an oxygen termination on the surface. The convergence was tested with respect to the number of layers, vacuum size, and *k*-points. For calculations of the adsorption energy, a slab with four composite layers was used, and a vacuum of 20 Å was added to minimize interactions between periodic images. The slab was then relaxed, using a gamma Γ-centered *k*-point mesh of 3×3×3. The bottom layer was fixed, while the second to the bottom layer was partially fixed (or, "semi-fixed") with atoms being free to relax along the *z*-direction only (see Fig. S10A). The rest atoms near the surface (*i.e.* atoms in the top two layers) are free to relax in the x, y and z directions. The lattice shape and volume were held constant. To avoid the interaction between adsorbent molecules with their periodic images, a (2×2×1) supercell was constructed with the optimized slab and further relaxed to obtain $E_{surface}$ for ZnO_2.

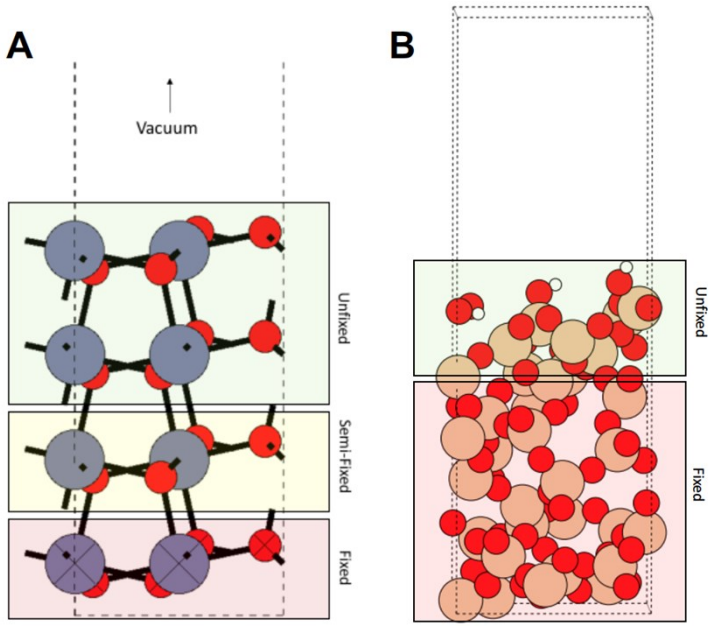

Fig. S11: Schematic showing which atoms are "fixed", "semi-fixed", and "unfixed" during the structure optimization of the ZnO_2 (A) and SiO_2 (B) surface slabs.

The amorphous SiO_2 nanoparticle surface was prepared in a multistep process. Our method follows closely to the one described by Ewing *et al*. which used a combination of MD and DFT simulations to model an amorphous SiO_2 surface.[11] Our MD calculations were performed using the large-scale atomic/molecular massively parallel simulator (LAMMPS)[12] with the Tersoff interatomic potential by Munetoh *et al*.[13] To create an amorphous SiO_2 structure, a crystalline structure was supercooled using

MD. A face center cubic SiO_2 supercell containing 96 atoms was used as our starting structure. The system was first heated to temperature of 5,000 K and it was equilibrated for 500 ps. The system was then rapidly cooled to 300 K at a rate of -0.47 K/ps and held for 100 ps. The structure from MD simulation was then further optimized by DFT including the atomic positions and cell parameters to create a bulk amorphous SiO_2. A surface was then created by removing atoms at the top and adding a vacuum of 15 Å along surface normal. As the resulted surface contains undersaturated/undercoordinated silicon and oxygen atoms, the surface was subsequently functionalized with silanol (Si-O-H) groups by attaching additional oxygen and hydrogen atoms to the undersaturated Si and O atoms. The atomic positions and cell parameters were then relaxed (see the setup in Fig. S10B) by DFT to determine $E_{surface}$ (SiO_2) where the atomic force convergence threshold was set to 0.02 eV/Å and the electronic energy convergence threshold is set to 10^{-4} eV.

Finally, $E_{surface+acetone}$ was calculated by adding an acetone molecule near the surface of the optimized ZnO_2 and a-SiO_2 slabs. The various potential binding sites were identified by systematically varying and exploring various lateral position and rotation of the acetone molecule relative to the surface. During relaxation, the acetone molecule was free to relax into any nearby stable binding sites. In most simulations, the acetone molecule will converge on the lowest-energy binding site. DFT predicts that acetone preferentially binds to the ZnO_2 (100) surface around the Zn site and the E_{ads} is -0.34 ±0.011. In the case of a-SiO_2, the E_{ads} of acetone on SiO_2 surface is close to -0.33±0.16 eV. The calculated adsorption energies suggest a relatively strong physisorption. The bonding in a-SiO_2 is most likely via hydrogen bonding between the carbonyl O and the silanol functional groups.

Brunauer-Emmett-Teller (BET) and vapor sorption isotherm results:

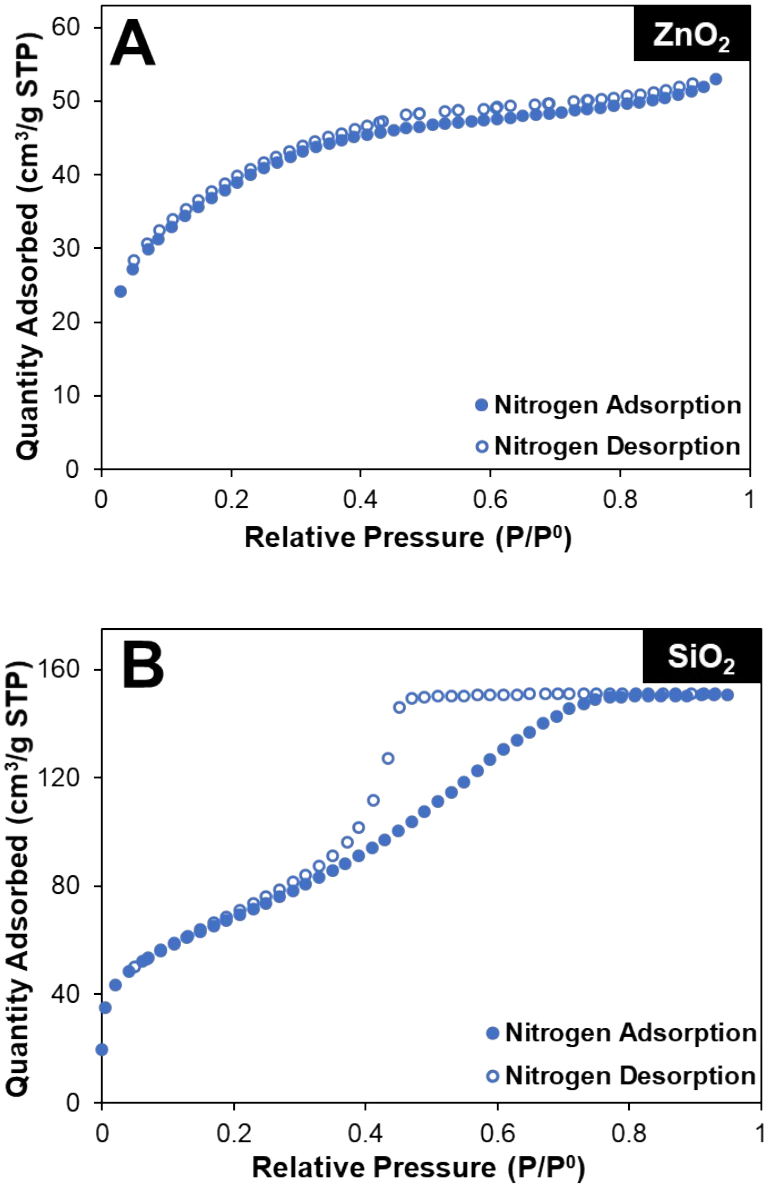

Fig. S12: Nitrogen adsorption analysis of the ZnO_2 nanoparticles. The calculated surface area via the BET method is 142.6 m^2/g. The shape of the isotherm is consistent with the formation of nonporous nanoparticles. Nitrogen adsorption analysis of the SiO_2 nanoparticles (B): the calculated surface area via the BET method is 246.9 m^2/g. The noticeable hysteresis in the isotherm is due to the presence of mesoporosity within the silica nanoparticles (B).

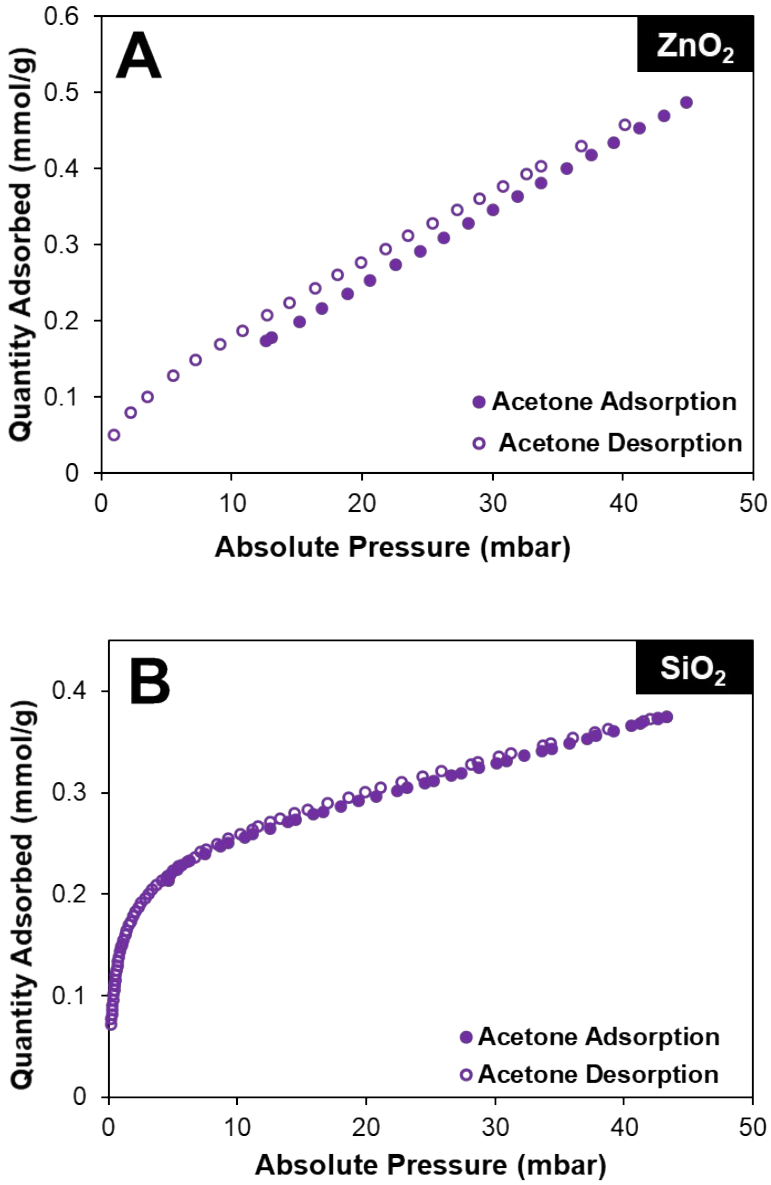

Fig. S13: Acetone adsorption isotherm for the ZnO_2 nanoparticles (A): the noticeable hysteresis between the adsorption and desorption curves is related to the strength of the acetone-ZnO_2 interaction. The adsorption likely consists of strong physisorption related to the preferential interaction of acetone to Zn sites. Acetone adsorption isotherm for the SiO_2 nanoparticles (B): the lack of a noticeable hysteresis, as well as the lower total uptake (0.375 mmol/g vs 0.486 mmol/g for ZnO_2) suggests a slightly weaker interaction between SiO_2 and acetone as compared to the ZnO_2. The higher initial uptake (reaching over 0.2 mmol/g at 4.7 mbar as opposed to 17 mbar for ZnO_2) is related to the increased surface area of the SiO_2 compared to the ZnO_2.

References:

1. Hohenberg, P. & Kohn, W. Inhomogeneous electron gas. *Phys. Rev.* **136**, B864–B871 (1964).

2. Kohn, W. & Sham, L. J. Self-consistent equations including exchange and correlation effects. *Phys. Rev.* **140**, A1133–A1138 (1965).

3. Jain, A. *et al.* Commentary: The materials project: A materials genome approach to accelerating materials innovation. *APL Mater.* **1**, 11002 (2013).

4. Kresse, G. & Furthmüller, J. Efficiency of ab-initio total energy calculations for metals and semiconductors using a plane-wave basis set. *Comput. Mater. Sci.* **6**, 15–50 (1996).

5. Kresse, G. & Furthmüller, J. Efficient iterative schemes for ab initio total-energy calculations using a plane-wave basis set. *Phys. Rev. B - Condens. Matter Mater. Phys.* **54**, 11169–11186 (1996).

6. Perdew, J. P., Burke, K. & Ernzerhof, M. Generalized gradient approximation made simple. *Phys. Rev. Lett.* **77**, 3865–3868 (1996).

7. Neugebauer, J. & Scheffler, M. Adsorbate-substrate and adsorbate-adsorbate interactions of Na and K adlayers on Al(111). *Phys. Rev. B* **46**, 16067–16080 (1992).

8. Bengtsson, L. Dipole correction for surface supercell calculations. *Phys. Rev. B - Condens. Matter Mater. Phys.* **59**, 12301–12304 (1999).

9. Ong, S. P. *et al.* Python Materials Genomics (pymatgen): A robust, open-source python library for materials analysis. *Comput. Mater. Sci.* **68**, 314–319 (2013).

10. Sun, W. & Ceder, G. Efficient creation and convergence of surface slabs. *Surf. Sci.* **617**, 53–59 (2013).

11. Ewing, C. S., Bhavsar, S., Veser, G., McCarthy, J. J. & Johnson, J. K. Accurate amorphous silica surface models from first-principles thermodynamics of surface dehydroxylation. *Langmuir* **30**, 5133–5141 (2014).

12. Plimpton, S. Fast parallel algorithms for short-range molecular dynamics. *J. Comput. Phys.* **117**, 1–19 (1995).

13. Munetoh, S., Motooka, T., Moriguchi, K. & Shintani, A. Interatomic potential for Si-O systems using Tersoff parameterization. *Comput. Mater. Sci.* **39**, 334–339 (2007).